Accuracy of SPECT/CT-based lung dose calculation for Holmium-166 hepatic radioembolization before OSEM convergence

Bastiaan J. van Nierop, Jip F. Prince,[a] Rob van Rooij, Maurice A.A.J. van den Bosch, Marnix G.E.H. Lam, and Hugo W.A.M. de Jong
Department of Radiology and Nuclear Medicine, University Medical Centre Utrecht, P.O. Box 85500, Utrecht, GA 3508, The Netherlands

(Received 27 October 2017; revised 26 April 2018; accepted for publication 14 May 2018; published 29 June 2018)

Purpose: In intra-arterial hepatic radioembolization using Holmium-166 (^{166}Ho) microspheres, a predicted lung-absorbed dose of more than 30 Gy is a contraindication for therapy. Therefore, scout imaging by means of quantitative SPECT of the lungs after a low-dose pretreatment session is essential. Earlier we showed the superiority of Monte Carlo-based iterative SPECT reconstructions over conventional reconstructions due to its quantitative nature, required for dosimetry, at the cost of substantial computation times. In clinical routine, however, the limited available time between scout imaging and therapy constrains its application. To reduce computation times, we investigated the minimum number of iterations required to guarantee a clinical acceptable accuracy in lung dose estimation using patient and phantom data.
Methods: ^{166}Ho scout SPECT data (range: 222-283 MBq) were used from 10 patients. SPECT images were Monte Carlo-based OSEM reconstructed (effective iterations: 240). Additionally, the 4D XCAT anthropomorphic phantom was used to mimic studies with an injected scout activity of 250 MBq and with varying lung-absorbed doses ranging from 0.9 to 225 Gy for a therapeutic dosage of 15 GBq. These studies were reconstructed in the same way as the patient data, and were also reconstructed using a clinically available, standard OSEM algorithm for comparison. Lung-absorbed dose was determined using VOI analysis as a function of iterations.
Results: The estimated lung-absorbed dose in nine patients ranged upon MC-based OSEM convergence from 0 to 0.26 Gy for a therapeutic dosage. One patient had an estimated lung absorbed-dose for a therapeutic dosage of 20.3 Gy upon MC-based OSEM convergence, or 18.4 Gy after 40 iterations (−9%). The phantom data showed that the lung-absorbed dose upon OSEM convergence was underestimated by 15% as compared to the actual simulated lung dose, and the dose after 40 iterations was underestimated by 9% as compared to the dose upon convergence. Both underestimations were irrespective of the magnitude of the lung-absorbed dose (0.9 to 225 Gy) and thus can be easily corrected for. The quantitative accuracy of the MC-based OSEM reconstructions (40 iterations, before convergence) outperformed the clinical OSEM reconstruction while estimating the lung dose.
Conclusions: The number of effective iterations necessary for quantitative estimation of the lung dose using MC-based OSEM can be reduced from 240 to 40. The resulting sixfold reduction in calculation time enables processing of the scout images before therapy administration. © *2018 The Authors. Medical Physics published by Wiley Periodicals, Inc. on behalf of American Association of Physicists in Medicine.* [https://doi.org/10.1002/mp.13024]

Key words: Holmium-166 microspheres, interventional oncology, iterative reconstruction, quantitative SPECT, radioembolization

1. INTRODUCTION

During intra-arterial radioembolization procedures, microspheres are injected in the hepatic artery for treatment of hepatic malignancies.[1] The microspheres may partially shunt from the hepatic artery to the hepatic vein after which they become lodged in the lungs, potentially causing radiation-induced lung disease, also referred to as radiation pneumonitis. To prevent this, pretherapy dosimetry based on a scout dosage microspheres, that is, administered shortly before the treatment dosage, should guide clinical decisions regarding the therapeutic activity administration.[2]

The standard clinical work-up in yttrium-90 (^{90}Y)-microsphere radioembolization consists of a prophylactic coil-embolization of nontarget vessels, followed by infusion of technetium-99 m (^{99m}Tc) macro-aggregated albumin (MAA) particles (Mallinckrodt Medical) and a SPECT/CT scan to assess the ^{99m}Tc-MAA distribution volume. If this so-called scout image does not reveal an unacceptable lung shunt with an associated high estimated absorbed lung dose from therapy (30 Gy in case of TheraSpheres™, or 20% lung shunt fraction in case of SirSpheres™), patients are scheduled for ^{90}Y radioembolization. This procedure is criticized because the MAA particles may exhibit a different

distribution as compared to the therapeutic microspheres, limiting the accuracy of the lung-absorbed dose estimation.[2]

Alternatively, when using ^{166}Ho the same particle is used for scout imaging (based on the emitted 81 keV photons) as for the therapy itself (based on the 1.77 and 1.85 MeV beta particles). This has the hypothetical advantage of a more reliable lung-absorbed dose estimation. To this end, first a ^{166}Ho-microsphere (QuiremSpheres™) scout dosage (approximately 250 MBq) is administered on the treatment day, followed by a SPECT/CT scan. The treatment dose is administered the same day a few hours later, but only if deemed safe based on the SPECT/CT scan. Estimation of the lung dose (expressed as mGy/MBq) from the scout dosage distribution enables a direct evaluation of the expected lung dose (Gy) resulting from the intended therapy.

Accurate dosimetry requires quantitative 3D image reconstruction of the scout dosage microsphere distribution in favor of 2D scintigraphy which may result in an overestimated lung dose.[2] There is general consensus that model-based iterative reconstruction yields the most accurate 3D images albeit at the cost of long reconstruction times. Earlier we reported that ^{166}Ho SPECT can accurately be reconstructed using Monte Carlo-based reconstructions requiring 240 iterations to converge, typically taking up to 2 h.[3] In daily clinical routine, however, the limited time available between scout and therapy activity administration constrains available calculation time. Reduction in the number of iterations is a well-known, straightforward way to reduce computation time, but it is unknown how this impacts lung dosimetry.

In this study, we explored the applicability of SPECT reconstructions with less iterations to perform lung dosimetry after a ^{166}Ho-microspheres administration. This was evaluated in patients and, to study the impact of a larger range of clinical situations on lung dosimetry, a set of anthropomorphic phantoms was also included.

2. MATERIALS AND METHODS

2.A. SPECT data acquisition

The ethics review board waived the need for informed consent of this retrospective study. Upon inspection of all patients (n = 80) with unresectable liver malignancies treated with ^{166}Ho-microspheres in our center (2011–2016) in the HEPAR-I, HEPAR-II, HEPAR-PLUS, and SIM trail, one patient was identified who presented an eminent lung shunt following the ^{166}Ho-microspheres scout dosage. For practical reasons the first nine, consecutive patients from the HEPAR-II trail were also included, that all did not present a lung shunt. Therefore, SPECT data of a total of 10 patients who underwent ^{166}Ho-microsphere scout imaging were retrospectively analyzed (Supporting Information Table S1) (total ^{166}Ho activity at the time of scanning: 222–283 MBq, Veenstra dose-calibrator, type VDC-404). Data were acquired on a dual-head Symbia T16 scanner (Siemens Healthcare, Germany), using 120 projections (energy window: 74.9–87.1 keV; acquisition time: 30 s per projection) over a noncircular 360° orbit, along with a breath-hold CT-derived attenuation map (Fig. 1).

2.B. SPECT reconstruction

Quantitative SPECT images were reconstructed using the Ordered Subset Expectation Maximization (OSEM) Utrecht Monte Carlo System (UMCS) within an iterative reconstruction algorithm (incorporating Monte Carlo-based scatter correction, attenuation correction, and modeling of photon interactions with the collimator and detector), as previously described.[3–5] Briefly, for each forward projection 1.000.000 photons were sampled from the full ^{166}Ho energy spectrum (0–2000 keV), including 14 of the most abundant gamma peaks as well as the Bremsstrahlung spectrum resulting from the interaction of two of the high-energy beta particles (Emax = 1.77 MeV, 0.49 cps/Bq; 1.85 MeV, 0.50 cps/Bq). After photon emission, Monte Carlo simulations of photon transport were done (primaries, scatter, and attenuation). The collimator-detector response was precalculated using MCNPX and was energy- and depth dependent. The optimum number of OSEM iterations for activity quantitation was based on previous work [number of iterations: 30, number of subsets: 8, equivalent to 240 Maximum Likelihood Expectation Maximization (MLEM) iterations].[3] The reconstruction time on a desktop computer (Windows 7, RAM: 20 GB, CPU: 3.3 GHz) was approximately 25 s per effective iteration, thus approximately 6000 s in total.

For comparison, a part of the anthropomorphic phantom data was also reconstructed using a widely available OSEM algorithm in the clinic (Flash3D, Siemens, Germany) using 30 iterations and 8 subsets for which the total reconstruction time was less than a minute. This reconstruction included attenuation correction and a window-based scatter correction (energy window: 110.9–125.1 keV). The scatter window was simulated using UMCS including Poisson noise. Finally, a k-factor of 1.15 was applied in the reconstruction, which was the ratio between (a) the number of counts in the photopeak window due to Bremsstrahlung, lead x rays and down-scatter from the high-energy (>81 keV) photons of ^{166}Ho, but not due to photons originating from the 81 keV photopeak, and (b) the number of counts in the upper scatter window due to Bremsstrahlung and down-scatter from the high-energy photons.

2.C. Anthropomorphic phantom

To study the impact of patient specifics on outcome, the digital 4D XCAT anthropomorphic phantom was used to simulate a series of attenuation maps and ^{166}Ho activity distributions (Fig. 1).[6] Simulations were performed with a male phantom (length: 181 cm; body weight: 87 kg), female phantom with underweight (length: 168 cm; body weight: 52 kg), female phantom with normal weight (length: 168 cm; body weight: 75 kg), and female phantom with overweight (length: 168 cm; body weight: 95 kg). End-expiratory lung volumes were 3049, 1775, 2885, and 3853 ml, respectively.

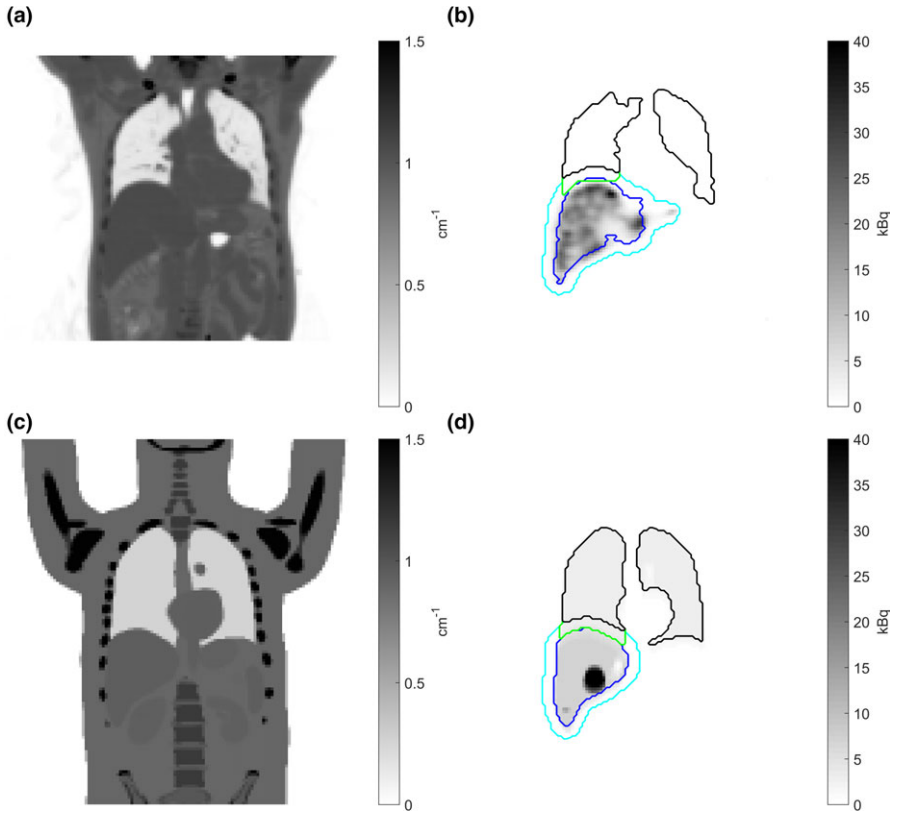

FIG. 1. Coronal cross-sections through a patient (male, 188 cm, 91 kg) (a, b) and through an anthropomorphic XCAT phantom (male, 181 cm, 87 kg) (c, d): CT-derived (a) and -simulated attenuation map (c) obtained at end-expiration for 81 keV photons; the corresponding cross-section of the reconstructed activity distribution using OSEM UMCS (b), with an estimated 0.1 MBq ^{166}Ho in the lungs and 269 MBq ^{166}Ho in the liver and liver lesions corresponding to a lung dose of 0 mGy/MBq; the corresponding cross-section of the simulated activity distribution (d), with 102 MBq ^{166}Ho in the lungs and 148 MBq ^{166}Ho in the liver and liver lesions corresponding to a lung dose of 4.8 mGy/MBq. Attenuation maps are scaled from 0 to 1.5 cm^{-1}, and activity distributions are scaled from 0 to 40 kBq. Indicated are the liver contour (blue line), liver + 2 cm contour (light blue line), lung contour (green line), and the lung contour without the overlapping region with the liver + 2 cm contour (black line), which was done in order not to count scatter from the liver as lung activity. [Color figure can be viewed at wileyonlinelibrary.com]

Simulations were done with a total of 250 MBq administered to the liver, liver tumors, and lungs. Tumors were represented by four spheres with diameters of 15, 20, 35, and 45 mm, with a fixed activity concentration ratio between tumors and liver tissue of 8:1.[7] The activity concentration ratio between the liver and lungs was varied, to resemble situations in which 0–74% of the activity shunted to the lungs, such that lung-absorbed doses were simulated up to an order of magnitude larger than the threshold for radiation pneumonitis, which is estimated to be 30 Gy.[8] Standard values in XCAT for a normal, respiration cycle were used with a respiration cycle of 5 s, a maximum diaphragm displacement of 2 cm and a maximum thorax expansion of 1.2 cm in the anterior–posterior direction. Time-averaged ^{166}Ho activity distributions and end-expiratory attenuation maps were used for simulations in accordance with the non-gated patient SPECT scans and breath-hold CT scans.

Monte Carlo simulations (using the in-house developed software package UMCS)[4,5] were used to obtain the projection images corresponding to noncircular orbit SPECT scans of the digital phantom (Supporting Information Fig. S1), resulting in images analogous to the patient images and with a similar number of counts per projection. Next, Poisson noise was added to the simulated projection images for which the number of counts in each pixel served as mean value λ. Finally, Monte Carlo-based OSEM reconstructions (OSEM UMCS) were used to reconstruct the simulated data, identical to the patient data (number of effective iterations: 240). Each simulation (male phantom only) was repeated ten times in order to determine the variance of the lung dose estimates. Finally, the male phantom data were also reconstructed using the standard OSEM algorithm (Flash3D).

2.D. Lung dose calculations

To determine the lung dose, volumes of interest (VOI) were defined to analyze the recovered activity in the liver and lungs as a function of effective iteration, both in the patient and simulated data. An expert reader (J.P.) obtained segmentations of the patient's liver (manually) and lungs (semi-automated) on CT data. The VOIs for the simulated data were directly obtained from the XCAT simulations. For both the patient and simulated data the liver volume was expanded by 2 cm to obtain a liver + 2 cm VOI, encompassing all scatter from the liver and blurring due to respiratory motion. Next, the overlapping region between the lung VOI and

liver + 2 cm VOI was excluded from the lung VOI in order to avoid counting scatter from the liver as lung activity (Fig. 1).[2] The activity in the lungs was estimated by multiplying the activity concentration in the lung VOI (excluding the liver + 2 cm VOI) with the volume of the total lung VOI.

From the quantitative reconstructed images (MBq), the lung dose (Gy) was calculated as previously described.[9] Briefly, the recovered activity (MBq) in the lungs was multiplied by the total energy released per unit of activity (15.87×10^{-3} J/MBq) (96% of the energy is emitted as beta radiation and deposited locally) and divided by the estimated lung mass (kg) assuming a lung tissue density of 0.3 g cm^{-3}. The estimated lung-absorbed dose (Gy) for the scout dosage was then normalized to the administered scout activity (MBq). This was done to enable straightforward comparison of the lung-absorbed dose to the threshold for radiation pneumonitis (30 Gy), based on the intended therapeutic activity (MBq), which was determined by dividing 60 Gy (the average dose to the liver tissue) by 15.87×10^{-3} J/MBq and multiplying by the liver mass (kg). Next the therapeutic activity is maximized to 15 GBq and reduced in the presence of a lung shunt.

2.E. Data analysis

Finally, the relation was determined between the estimated lung dose before convergence and the estimated lung dose upon convergence of the reconstruction algorithm (number of effective iterations: 240) using linear regression analysis with offset. For the anthropomorphic phantoms the relationship between the lung dose upon convergence of the reconstruction algorithm and the imposed lung dose was determined likewise.

Data analysis was performed in Matlab (The Mathworks, Natick, MA, USA), except for the segmentation of the patient's liver and lungs, which was done using in-house-developed software.[10] Statistical analysis was performed using SPSS 22.0 (SPSS Inc., Chicago, IL, USA), for which the level of significance was set at $\alpha = 0.05$.

3. RESULTS

Figure 2 shows the reconstructed activity distributions for the simulated and reconstructed activity distributions for the XCAT data (without and with a lung shunt) and for the patient data at multiple numbers of effective iterations. After eight effective iterations the shape and position of the liver and large liver lesions can be recognized, but the activity distributions appear blurred, both in the patient and simulated data. Increasing number of iterations result in increased contrast at the cost of increased noise.

In nine patients, the estimated lung-absorbed dose (normalized to the administered scout activity) was 0.01 mGy/MBq as determined from the reconstructed activity distribution upon convergence of the reconstruction algorithm (number of effective iterations: 240) (Fig. 3), whereas one patient had an estimated lung dose of 1.35 mGy/MBq [Figs. 2(c), Fig. 3]. This latter dose corresponds to an estimated lung dose of 20.3 Gy for a therapeutic dosage of 15 GBq, which remained below the estimated threshold for radiation pneumonitis (30 Gy). In this patient, the estimated lung dose was 1.22 mGy/MBq after 40 effective iterations, corresponding to an underestimation of 9.3%.

The estimated lung dose as a function of effective iteration in the anthropomorphic phantoms without a lung shunt showed essentially the same trend as in the nine patients without a lung shunt (Fig. 3). In all phantoms, the estimated lung-absorbed dose ranged from 0.004 to 0.008 mGy/MBq as determined from the reconstructed activity distribution upon convergence of the reconstruction algorithm. After 40 effective iterations the estimated dose ranged from 0.03 to 0.07 mGy/MBq, or 0.45 to 1.1 Gy for a therapeutic dosage.

The estimated lung dose in the simulated data after 240 effective iterations was linearly correlated with the estimated dose after 8, 16, 24, 32, and 40 effective iterations (Pearson correlation coefficient $r = 0.99$, $P < 0.001$, in all cases) (Fig. 4). The lung-absorbed dose as estimated after 8, 16, 24, 32, and 40 effective iterations was underestimated by 38%, 22%, 15%, 12%, and 9%, respectively, as compared to the estimated dose upon convergence of the OSEM algorithm. Importantly, the estimated lung-absorbed dose upon OSEM convergence was underestimated by 15% as compared to the actual simulated lung dose (Pearson correlation coefficient $r = 0.99$, $P < 0.001$) (Fig. 5). Both underestimations were irrespective of the magnitude of the lung dose. The estimated lung dose in the male phantoms when using 40 effective iterations with the Monte Carlo-based OSEM algorithm (before convergence) better resembled the imposed lung dose than when using the clinically available OSEM algorithm using 240 effective iterations (upon convergence) (Fig. 6).

The estimated lung dose in the anthropomorphic phantoms with a substantial lung shunt rapidly converged to the dose as estimated based on the activity distribution upon convergence of the algorithm (Fig. 7). In these simulations, the estimated lung-absorbed dose ranged from 0.06 to 15 mGy/MBq as determined from the reconstructed activity distribution upon convergence of the reconstruction algorithm. This corresponds to an estimated lung dose of 0.9–225 Gy for a therapeutic dosage of 15 GBq. After 40 effective iterations, the estimated dose ranged from 0.06 to 13.9 mGy/MBq, or 0.9–208.5 Gy for a therapeutic dosage.

4. DISCUSSION

Typically, the number of iterations for reconstruction of SPECT data is chosen such that sufficient resolution is recovered over the entire field of view with acceptable levels of noise (after filtering), for example, in order to detect small lesions.[11,12] In contrast, it is typically assumed that a lung shunt during radioembolization therapy results in a mostly homogeneous exposure of lung tissue to the microspheres,[13] loosening the demands for resolution recovery. This motivated us to investigate the quantitation of lung-absorbed dose from SPECT data using as few iterations as possible while

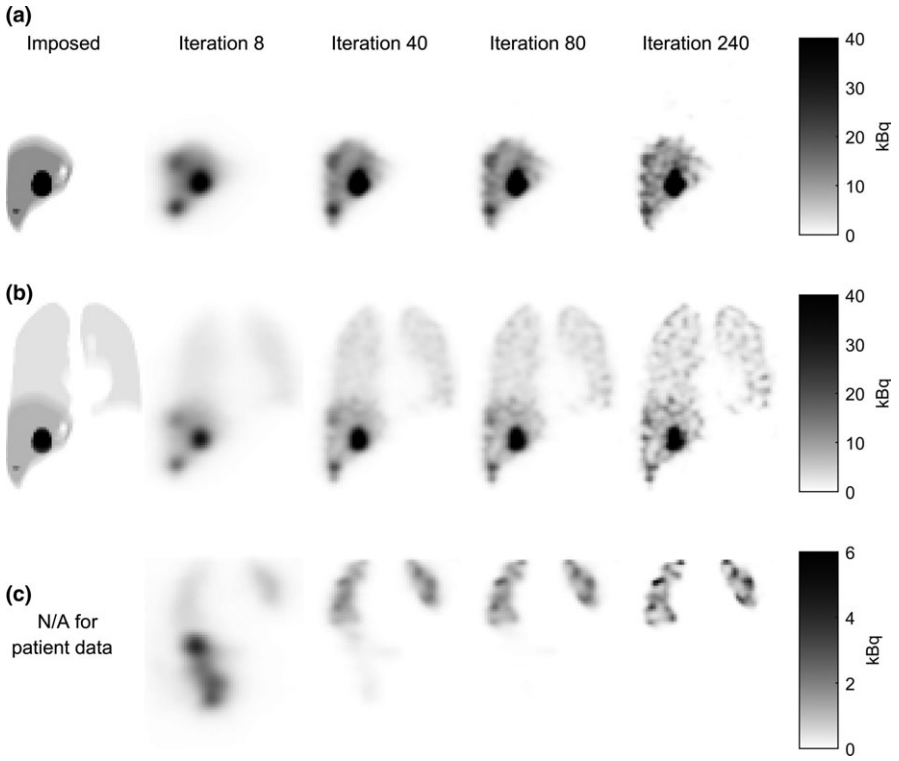

FIG. 2. OSEM UMCS reconstruction of an anthropomorphic phantom with a lung dose of 0.08 mGy/MBq (a; imposed liver and lung activity 247 MBq and 3 MBq, respectively; images scaled from 0 to 40 kBq) and a lung dose of 4.8 mGy/MBq (b; imposed liver and lung activity 148 and 102 MBq, respectively; images scaled from 0 to 40 kBq) and of a patient with an estimated lung dose of 1.35 mGy/MBq (c; estimated lung activity 10 MBq; images scaled from 0 to 6 kBq). Note that in this patient only the anterior part (section 4B) of the liver was treated. The coronal section shown in 2C does not intersect with this part of the liver such that with the algorithm converging the activity disappears from the coronal section shown. From left to right the imposed activity distribution, the OSEM UMCS reconstruction after 8, 40, 80, and 240 effective iterations.

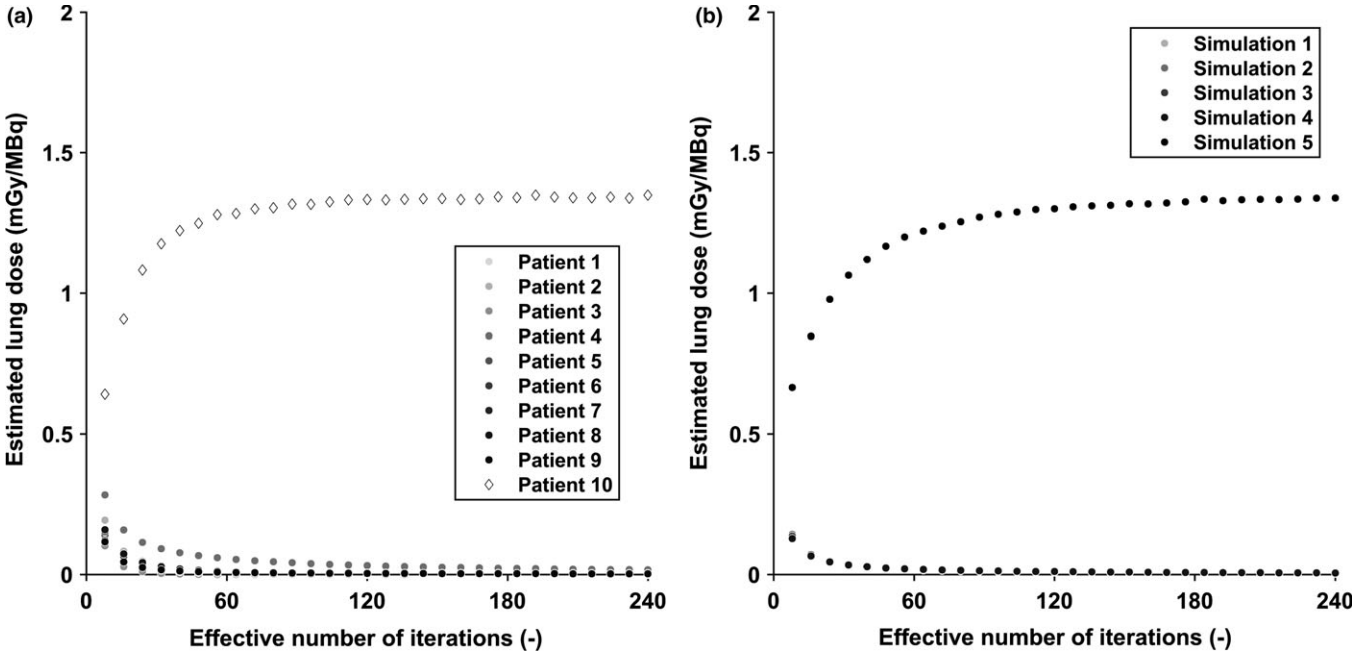

FIG. 3. Estimated lung dose (Gy/MBq) using OSEM UMCS as function of the effective iteration number for the patient data with a very small (1–9) and with (10) a substantial lungshunt (a) and for four anthropomorphic phantoms without and one with a lung shunt (b). The estimated lung dose in the patient with a lung shunt was 1.35 mGy/MBq upon convergence of the reconstruction algorithm (number of effective iterations: 240). The estimated dose ranged from 0 to 0.025 mGy/MBq for all patients with a very small lung shunt (number of effective iterations: 240). The estimated lung dose in the anthropomorphic phantoms without a lung shunt (one male, three females with varying bodyweight) showed essentially the same trend as for the patient data itself and ranged from 0.004 to 0.008 mGy/MBq upon convergence of the reconstruction algorithm.

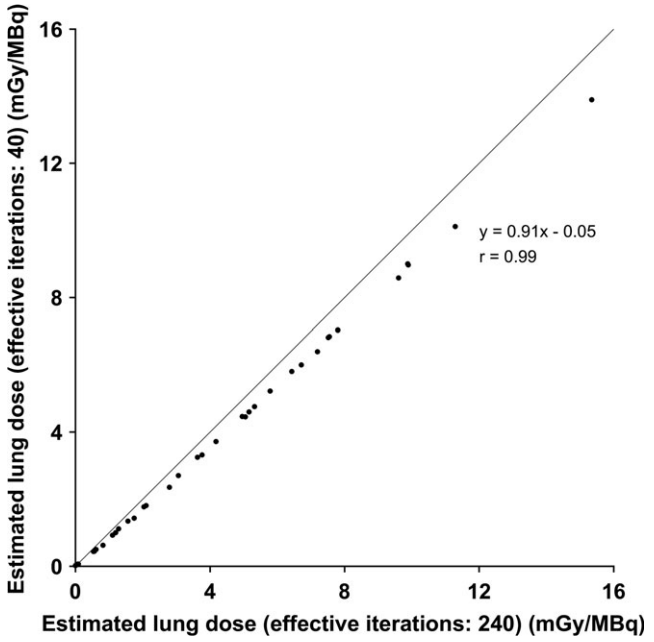

FIG. 4. The estimated lung dose (mGy/MBq) using OSEM UMCS of the anthropomorphic phantoms as estimated before convergence (number of effective iterations: 40) expressed as a function of the estimated lung dose upon convergence of the OSEM algorithm (number of effective iterations: 240). Note that a linear correlation was obtained between both (Pearson correlation coefficient $r = 0.99$, $P < 0.001$) and that the estimated dose after 40 iterations was 9% smaller than the estimated dose after 240 iterations. The line of unity is added to the plot.

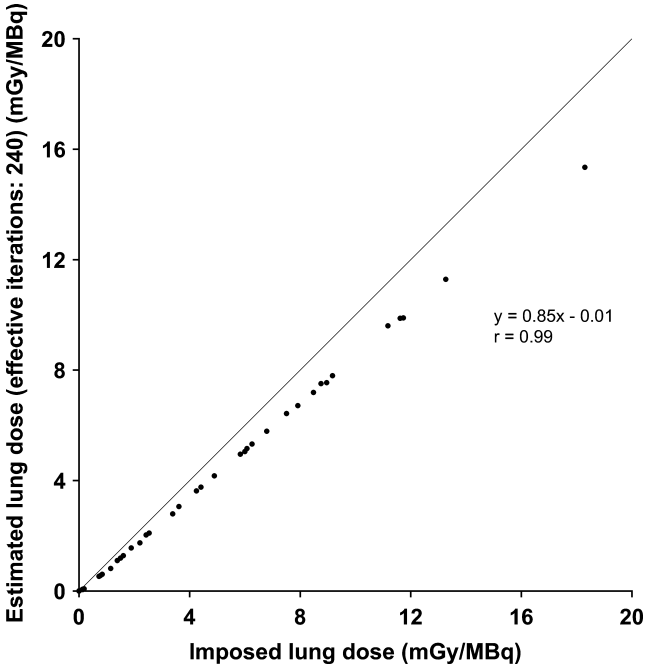

FIG. 5. The estimated lung-absorbed dose upon convergence of OSEM UMCS (mGy/MBq) (240 effective iterations) as a function of the imposed lung dose (mGy/MBq) in the anthropomorphic phantoms. Note that a linear correlation was obtained between both (Pearson correlation coefficient $r = 0.99$, $P < 0.001$) and that the estimated dose after 240 iterations was 15% smaller than the imposed dose. The line of unity is added to the plot.

not compromising the detection of a potentially hazardous lung shunt. Although in-house-developed reconstruction software was used to this end, the underlying OSEM algorithm is generally available making the conclusion relevant to other reconstruction tools using the OSEM algorithm as well. For example for the Monte Carlo-based reconstruction of ^{90}Y Bremsstrahlung SPECT images in the setting of liver radioembolization.[14,15]

Results from this study indicate that 40 effective iterations suffice to quantitate the lung-absorbed dose after ^{166}Ho-microspheres administration without compromising the clinical decision-making concerning a potentially harmful lung-absorbed dose. This enables quantitation of the ^{166}Ho scout dosage distribution before therapy administration on the same day in an acceptable 15 min for lung dose calculation and approximately 15 min for the lung segmentation, which is of special importance for future studies lacking a ^{99m}Tc-MAA scout dosage. Although in the presence of a lung shunt the sixfold reduction in the number of iterations results in a 9% underestimation of the lung dose, this effect was irrespective of the activity in the lungs. Therefore, this underestimation can simply be accounted for when calculating the maximum acceptable therapeutic dosage without exceeding the threshold dose for radiation pneumonitis.

Alternatively, the possibility was explored to use a widely available OSEM algorithm with window-based scatter correction requiring less calculation time until convergence than OSEM UMCS (using 40 effective iterations). To this end an

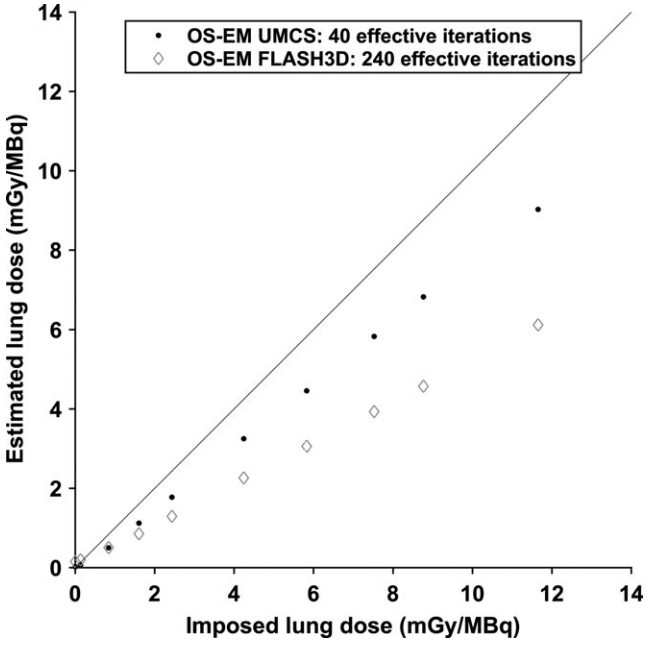

FIG. 6. Estimated lung dose (mGy/MBq) of the different male, anthropomorphic phantoms with varying imposed lung activity as a function of the imposed lung dose (mGy/MBq), for the Monte Carlo-based OSEM UMCS algorithm using 40 effective iterations (black dots, before convergence of the algorithm) and the clinically available OSEM algorithm Flash3D using 240 effective iterations (gray diamonds, upon convergence of the algorithm). The line of unity is represented by the black line. Note that the underestimation of the imposed lung dose is smaller when using OSEM UMCS than when using the Flash3D algorithm.

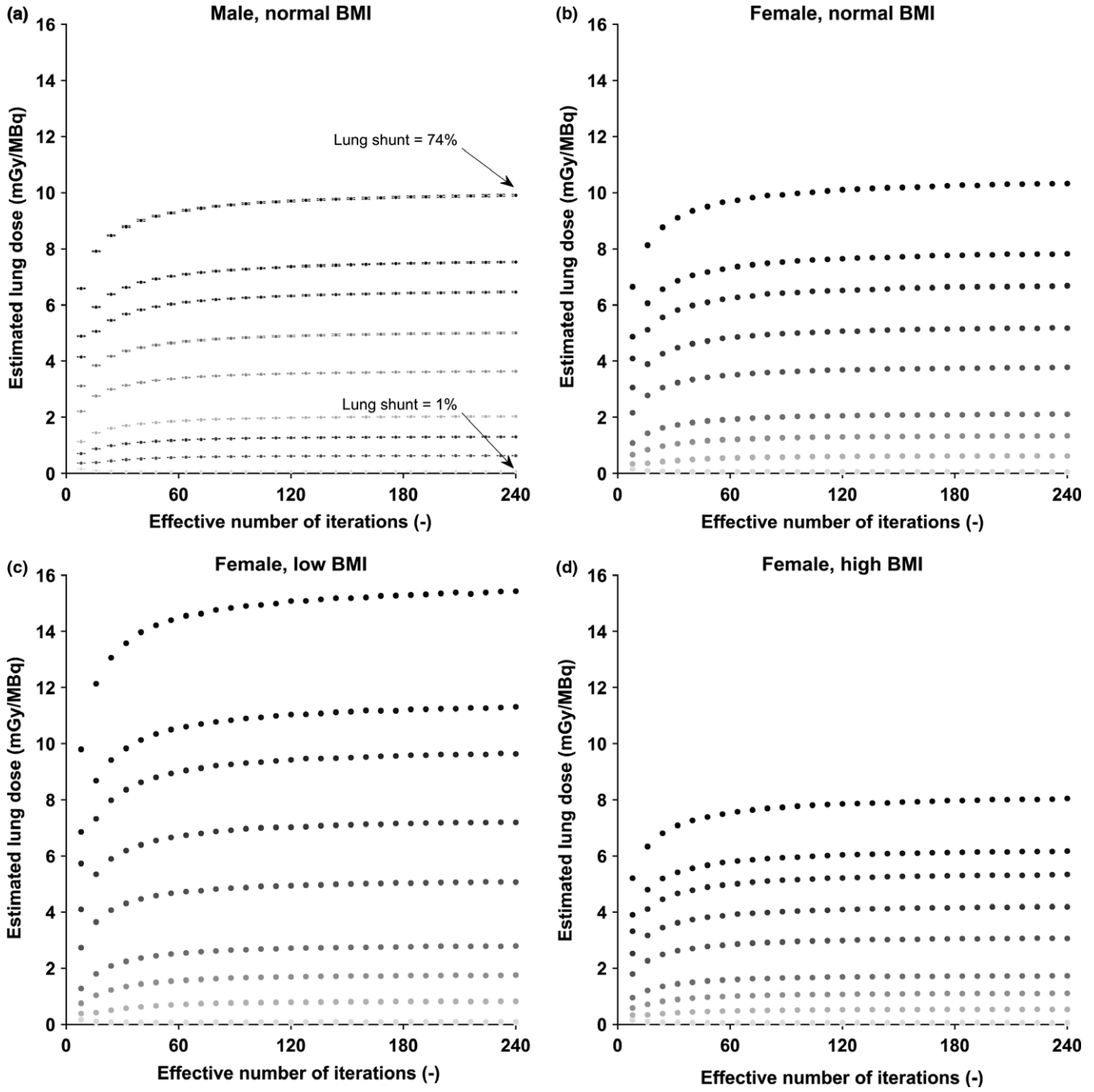

FIG. 7. The estimated lung dose expressed as mGy/MBq as a function of effective iteration number for the simulated male phantom (a), female with normal weight (b), female with underweight (c), and female with overweight (d). Simulated lung shunts in each panel range from 1% to 74%. Note that the resulting, estimated lung dose varied as a result of differences in body mass. In Supporting Information Fig. S2 the same data are represented, but then expressed as recovered activity (MBq) in the lungs normalized to the imposed activity (MBq) instead of the estimated lung dose (mGy/MBq). For the male phantom the mean and standard deviation are represent by dots and error bars.

upper scatter window was used. A triple energy window approach was deemed unsuitable as the ^{166}Ho spectrum just below the 81 keV photopeak window also contains x-ray emissions around 49 keV as well as lead x rays formed in the collimator around 74 keV. However, the upper scatter window can only be used to estimate Bremsstrahlung and downscatter from high-energy photons in the photopeak window. On the other hand, all relevant photon interactions are taken into account in the Monte Carlo-based reconstruction. An OSEM algorithm with window-based scatter correction is, therefore, expected to underperform in terms of quantitative accuracy as compared to an OSEM algorithm with Monte Carlo-based scatter correction. Indeed, even before convergence OSEM UMCS outperformed the standard OSEM algorithm in terms of quantitative accuracy while estimating the lung dose.

Importantly, the estimated lung dose upon OSEM convergence underestimated the actual simulated lung dose by

another 15% (Fig. 5). Following clinical practice, the VOIs used to quantitate the total lung activity were defined on a breath-hold CT scan, whereas the SPECT scans were acquired under continuous breathing. Due to the resulting partial volume effects the activity concentration near the edge of the lungs as observed on the reconstructed images will be underestimated (Supporting Information Fig. S3). This in turn causes the underestimation of the lung-absorbed dose. This effect was irrespective of the number of microspheres shunted to the lungs and should thus be corrected for, in addition to the correction for the underestimation resulting from reduction in the number of iterations. Alternatively, the lung VOI can be compressed omitting the edges of the lungs while estimating the lung activity concentration.

Nine patients included in this study had a negligible estimated lung dose as quantified from the ^{166}Ho scout dosage distribution upon convergence of the OSEM algorithm. This is probably due to the fact that none of these patients had hepatocellular carcinoma. Patients with hepatocellular carcinoma are most likely to present a lung shunt.[16] In these patients, the absence of a substantial lung shunt also became apparent from a visual inspection of the reconstructed data after the eight effective iterations onwards, but was more obvious after 40 effective iterations. Indeed, after 40 effective iterations the estimated lung-absorbed dose for a therapeutic dosage ranged from 0.03 to 1.17 Gy. One patient with hepatocellular carcinoma had a substantial lung shunt. In this patient, the presence of a lung shunt became apparent from visual inspection of the reconstructed data after eight effective iterations onwards, but was more obvious after 40 effective iterations. The estimated lung-absorbed dose was 18.4 and 20.3 Gy after 40 and 240 effective iterations, respectively.

Extrapolation of the conclusions drawn from the patient data to a broader patient population with potentially varying activity distribution was precluded, as the number of patients included was limited and their estimated lung doses were far below the estimated threshold for radiation pneumonitis. Simulations were, therefore, performed to validate these results for a patient population with higher lung shunts and to investigate the convergence of the iterative reconstruction algorithm for varying activity distributions, as these are known to affect the number of iterations required.[17] For this the digital 4D XCAT anthropomorphic phantom was used, which provides an excellent model to answer questions regarding emission tomography studies that are hard to study otherwise.[6,18–21]

In this study, the number of iterations was minimized as a means to reduce the calculation time of the Monte Carlo-based OSEM algorithm while still guaranteeing a clinically acceptable accuracy in lung dose estimation. This approach is complementary to other means to decrease computation times, such as parallel computing, which all fit in the continuous efforts made to accelerate reconstruction algorithms. The results from our study might also be applicable to other situations in which SPECT data are reconstructed of essentially homogeneous activity distributions or when the recovery of smaller structures is of less importance, such as ventilation/perfusion SPECT.[22]

5. CONCLUSION

The number of iterations necessary for estimating the lung dose from a ^{166}Ho scout dosage SPECT scan when using quantitative, Monte Carlo-based reconstructions can be reduced from 240 to 40 effective iterations. The resulting sixfold reduction in calculation time enables data processing of the ^{166}Ho scout scan before therapy administration in future studies lacking a ^{99m}Tc scout scan to assess therapy safety.

Partial volume effects, merely due to respiratory motion, result in an underestimation of the estimated lung dose (mGy/MBq) of 15% as compared to the actual lung dose and the use of 40 effective iterations results in an additional 9% reduction as compared to the estimated lung dose upon convergence of the OSEM algorithm. Both effects are irrespective of the magnitude of the lung shunt. When calculating the maximum therapeutic activity these underestimations should be accounted for in order to not compromise the detection of potentially hazardous lung shunts and to remain below the radiation pneumonitis threshold.

ACKNOWLEDGMENT

The authors thank G.H. Bol for his assistance with the software used to segment the patient's liver and lungs. This project has received funding from the European Research Council (ERC) under the European Union's Horizon 2020 research and innovation programme (grant agreement No [646734]).

CONFLICTS OF INTEREST

ML is a consultant for Sirtex, BTG, and Mirada. The department of Radiology and Nuclear Medicine of the UMC Utrecht receives royalties from Quirem Medical BV. All other author(s) declare that they have no competing interests.

[a]Author to whom correspondence should be addressed. Electronic mail: b.j.vannierop@umcutrecht.nl; Telephone: +31 (0)88 7553258.

REFERENCES

1. Andreana L, Isgro G, Marelli L, et al. Treatment of hepatocellular carcinoma (HCC) by intra-arterial infusion of radio-emitter compounds: trans-arterial radio-embolisation of HCC. *Cancer Treat Rev.* 2012;38:641–649.
2. Elschot M, Nijsen JF, Lam MG, et al. Tc-MAA overestimates the absorbed dose to the lungs in radioembolization: a quantitative evaluation in patients treated with Ho-microspheres. *Eur J Nucl Med Mol Imaging*. 2014;41:1965–1975.
3. Elschot M, Smits ML, Nijsen JF, et al. Quantitative Monte Carlo-based holmium-166 SPECT reconstruction. *Med Phys*. 2013;40:112502.
4. de Jong HWAM, Slijpen ETP, Beekman FJ. Acceleration of Monte Carlo SPECT simulation using convolution-based forced detection. *Ieee T Nucl Sci*. 2001;48:58–64.
5. Beekman FJ, de Jong HWAM, van Geloven S. Efficient fully 3-D iterative SPECT reconstruction with Monte Carlo-based scatter compensation. *Ieee T Med Imaging*. 2002;21:867–877.

6. Segars WP, Sturgeon G, Mendonca S, Grimes J, Tsui BM. 4D XCAT phantom for multimodality imaging research. *Med Phys*. 2010;37: 4902–4915.
7. Willowson KP, Tapner M, Bailey DL. A multicentre comparison of quantitative (90)Y PET/CT for dosimetric purposes after radioembolization with resin microspheres : the QUEST Phantom Study. *Eur J Nucl Med Mol Imaging*. 2015;42:1202–1222.
8. Yorke ED, Jackson A, Rosenzweig KE, Braban L, Leibel SA, Ling CC. Correlation of dosimetric factors and radiation pneumonitis for non-small-cell lung cancer patients in a recently completed dose escalation study. *Int J Radiat Oncol Biol Phys*. 2005;63:672–682.
9. Vente MA, Nijsen JF, de Wit TC, et al. Clinical effects of transcatheter hepatic arterial embolization with holmium-166 poly(L-lactic acid) microspheres in healthy pigs. *Eur J Nucl Med Mol Imaging*. 2008;35:1259–1271.
10. Bol GH, Kotte AN, van der Heide UA, Lagendijk JJ. Simultaneous multi-modality ROI delineation in clinical practice. *Comput Methods Programs Biomed*. 2009;96:133–140.
11. Liow JS, Strother SC. The convergence of object dependent resolution in maximum likelihood based tomographic image reconstruction. *Phys Med Biol*. 1993;38:55–70.
12. Liow JS, Strother SC. Practical tradeoffs between noise, quantitation, and number of iterations for maximum likelihood-based reconstructions. *IEEE Trans Med Imaging*. 1991;10:563–571.
13. Yu N, Srinivas SM, Difilippo FP, et al. Lung dose calculation with SPECT/CT for (9)(0)Yittrium radioembolization of liver cancer. *Int J Radiat Oncol Biol Phys*. 2013;85:834–839.
14. Porter CA, Bradley KM, Hippelainen ET, Walker MD, McGowan DR. Phantom and clinical evaluation of the effect of full Monte Carlo collimator modelling in post-SIRT yttrium-90 Bremsstrahlung SPECT imaging. *EJNMMI Res*. 2018;8:7.
15. Elschot M, Vermolen BJ, Lam MG, de Keizer B, van den Bosch MA, de Jong HW. Quantitative comparison of PET and Bremsstrahlung SPECT for imaging the in vivo yttrium-90 microsphere distribution after liver radioembolization. *PLoS ONE*. 2013;8:e55742.
16. Ward TJ, Tamrazi A, Lam MG, et al. Management of High Hepatopulmonary Shunting in Patients Undergoing Hepatic Radioembolization. *J Vasc Interv Radiol*. 2015;26:1751–1760.
17. Lyra M, Ploussi A. Filtering in SPECT Image Reconstruction. *Int J Biomed Imaging*. 2011;2011:693795.
18. Minarik D, Senneby M, Wollmer P, et al. Perfusion vector-a new method to quantify myocardial perfusion scintigraphy images: a simulation study with validation in patients. *EJNMMI Res*. 2015;5:121.
19. Konik A, Kupinski M, Pretorius PH, King MA, Barrett HH. Comparison of the scanning linear estimator (SLE) and ROI methods for quantitative SPECT imaging. *Phys Med Biol*. 2015;60:6479–6494.
20. Segars WP, Norris H, Sturgeon GM, et al. The development of a population of 4D pediatric XCAT phantoms for imaging research and optimization. *Med Phys*. 2015;42:4719–4726.
21. Konik A, Connolly CM, Johnson KL, et al. Digital anthropomorphic phantoms of non-rigid human respiratory and voluntary body motion for investigating motion correction in emission imaging. *Phys Med Biol*. 2014;59:3669–3682.
22. Roach PJ, Gradinscak DJ, Schembri GP, Bailey EA, Willowson KP, Bailey DL. SPECT/CT in V/Q scanning. *Semin Nucl Med*. 2010;40: 455–466.

SUPPORTING INFORMATION

Additional Supporting Information may be found online in the supporting information section at the end of the article:

Table S1. Characteristics of the HEPAR-II patients included in this study.

Figure S1. Anterior projection image of the patient in Fig. 1 (left). UMCS simulation of an anterior projection image obtained with the simulated attenuation map and activity distribution in Fig. 1 (right). Images are scaled from 0 to 50 counts.

Figure S2. The estimated lung activity normalized to the imposed lung activity (expressed as percentage) as a function of effective iteration number for the simulated male phantom (a), female with normal weight (b), female with underweight (c), and female with overweight (d). Simulated lung shunts in each panel range from 1% to 74%. Note that for very small lung shunts the activity in the lung in fact was overestimated after a small number of effective iterations as compared to the estimated activity upon convergence.

Figure S3. Example of a simulated, uniform activity distribution in the lungs with respiratory motion (left). The image is scaled from 0 to 40 kBq. Indicated are the liver contour (blue line), liver + 2 cm contour (light blue line), lung contour (red line), and the lung contour without the overlapping region with the liver + 2 cm contour (green line). The estimated lung-absorbed dose from the lung VOI (red line) (mGy/MBq) as a function of the number of OSEM iterations for a simulation with and without respiratory motion (right). Indicated is the imposed lung-absorbed dose (dotted line). Note that in the absence of motion the imposed lung-absorbed dose is obtained upon convergence of the reconstruction algorithm (effective number of iterations: 240), while in the presence of partial voluming due to respiratory motion the lung-absorbed dose is underestimated upon convergence.